Monochromatized Synchrotron Radiation at the MAX Beamline 52

DIPLOMA PAPER

Ola Widlund

Department of Physics,
Lund Institute of Technology

Lund Reports on Atomic Physics, LRAP-114
Lund, August 1990

Contents

1. Introduction

This diploma work has been performed in the spring of 1990 at the MAX laboratory in Lund, where I have been working on beamline 52 with a group from the department of Physics I at the Royal Institute of Technology in Stockholm (KTH).

Beamline 52 at MAX is equipped with a 1 m normal incidence monochromator designed by S. Huldt, U. Litzén and others in the Atomic Spectroscopy group at the University of Lund [13, 21]. The Stockholm group has proposed to use this instrument in a series of gas-phase experiments.

My work has been focussed mainly on the alignment and characterization of the monochromator at beamline 52, but I have also participated in the preparations for the intended gas-phase experiments.

1.1 THE REPORT

The first part of the report (Chapters 2 and 3) can be seen as a general introduction to the use of synchrotron radiation, but the interest is focussed mainly on the MAX storage ring and beamline 52 at MAX, respectively.

After an introduction to monochromators and grating theory in general in Chapter 4, the next two chapters deal with the 1 m normal incidence monochromator designed for beamline 52. Chapter 5 describes the design of the instrument and Chapter 6 deals with its performance.

Finally, Chapter 7 presents a very brief introduction to the gas-phase experiments scheduled for beamline 52.

1.2 ACKNOWLEDGEMENTS

First of all I would like to thank Stacey L. Sorensen for acting as my supervisor and "Boss", but most of all for being such a nice person to work with.

I would also like to thank the personnel at the MAX laboratory for their kind help and support and also for bringing delicious cakes for the coffee

breaks; Sverker Werin for introducing me to the gang of cross-country runners from Kalmar (?!).

Finally, I owe many thanks to Elisabeth Källne, Ulf Litzén, Prof. Sune Svanberg, Stacey Sorensen and a few of my friends for their detailed and constructive criticism of my manuscript.

2. Synchrotron Radiation

2.1 WHAT IS SYNCHROTRON RADIATION ?

It is well known that electrons submitted to an accelerating field emit electromagnetic waves. This is, for example, the case for a normal antenna, where the acceleration of the electrons is weak and the radiation emitted is in the radio frequency range.

In circular high-energy accelerators the electrons experience a very strong centripetal acceleration induced by the magnetic fields from the bending magnets. The electron energy can be as high as several giga electron volts (GeV) and in this energy range electrons are highly relativistic, i.e. their kinetic energy is much higher than the energy of an electron at rest, m_0c^2 (= 511 MeV). Figure 1, originating from Tomboulian and Hartman [1], shows the geometry of synchrotron radiation emitted by an electron in a circular orbit. We see how the dipole-like angular distribution of radiation from a slow electron (left) is distorted into a narrow cone in the direction of motion when the speed is close to that of light (right).

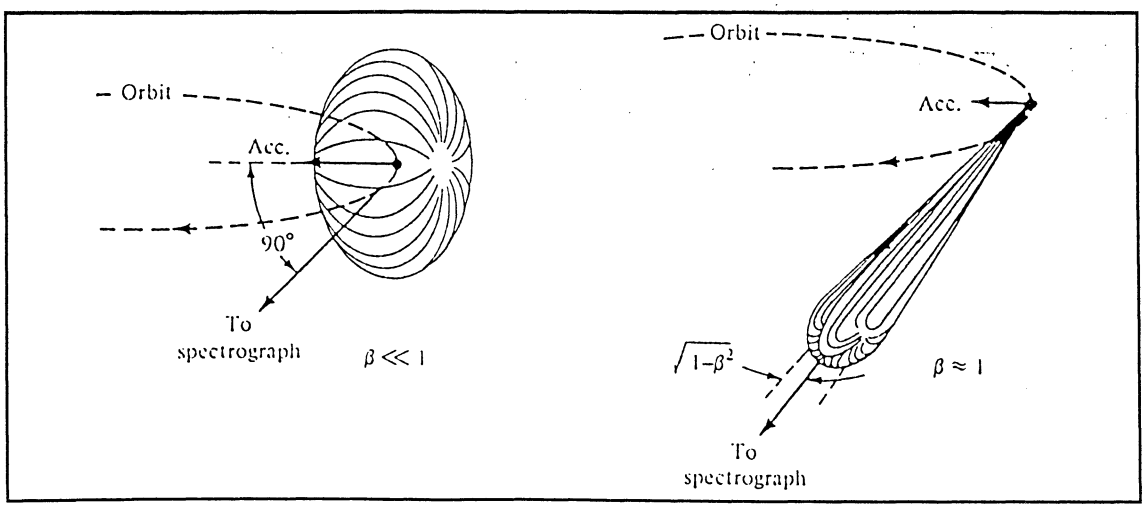

Fig. 1 Angular distribution of the emitted intensity for slow (left) and relativistic (right) electrons [2]. ($\beta = v/c$).

A description of the theory of synchrotron radiation can be found in a reference [2], that has been of great help to me, or in the original works of Schwinger [3 – 5] and others. We will not go deeper into this, but we will write down a few expressions that can be used for quantitative studies of

some of the properties of synchrotron radiation.

For relativistic, monoenergetic electrons in a circular orbit the total power radiated can be written as (SI units)

$$P = \int\int I(\lambda, \psi)\, d\lambda\, d\psi = \frac{2}{3}\frac{e^2 c}{4\pi\,\varepsilon_0\, R^2}\left(\frac{E}{mc^2}\right)^4, \tag{1}$$

where

$$I(\lambda, \psi) = \left[\frac{e^2 c}{4\pi\,\varepsilon_0\, R^3}\right]_{SI} T_{dip}\,\frac{27}{32\pi^3}\left(\frac{\lambda_c}{\lambda}\right)^4 \gamma^8 \left(1+\gamma^2\psi^2\right)^2 \left[K_{1/3}^{\,2}(\xi) + \frac{\gamma^2\psi^2}{1+\gamma^2\psi^2}\, K_{2/3}^{\,2}(\xi)\right] \tag{2}$$

and $$\xi \equiv \frac{\lambda_c}{2\lambda}\left(1+\gamma^2\psi^2\right)^{3/2}. \tag{3}$$

γ is the ratio of the kinetic energy to the rest-mass energy of an electron;

$$\gamma = \frac{E}{m_0 c^2}. \tag{4}$$

We define λ_c as the characteristic or critical wavelength given by

$$\lambda_c = \frac{4}{3}\,\pi\, R\, \gamma^{-3}. \tag{5}$$

λ is the wavelength for the emitted radiation and ψ is the azimuthal angle relative to the plane of orbit. $K_{1/3}(\xi)$ and $K_{2/3}(\xi)$ are modified Bessel functions of the second kind. The first and second terms in the bracket of (2) are connected to the polarization parallel and normal, respectively, to the plane of orbit.

The factor T_{dip} takes care of the fact that the electron only radiates in the dipole magnets with radius R and not in the straight sections of total length L.

$$T_{dip} = \frac{2\pi R}{2\pi R + L} \tag{6}$$

In Sect. 2.3 of this chapter, these equations have been used – with parameters appropriate to MAX – to demonstrate a few of the interesting properties of synchrotron radiation.

2.2 DESIGN OF THE MAX STORAGE RING

The design of the MAX storage ring has been optimized to give high performance at a relatively low cost [6]. The typical electron energy is 550 MeV and the characteristic wavelength 40 Å. The storage ring is built with eight dipole bending magnets, with a bending radius of 1.20 m (R), and eight straight sections of total length 32.4 m (L) (see Fig. 2).

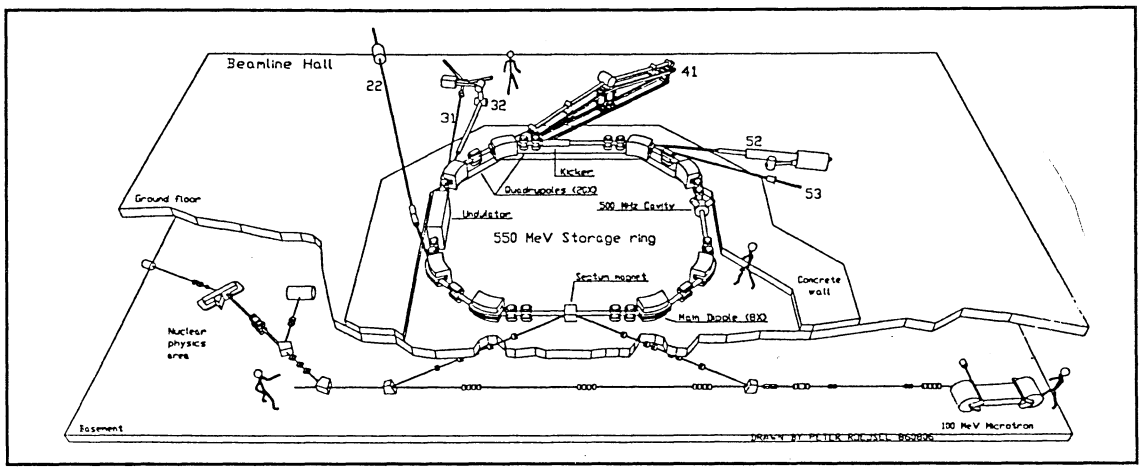

Fig. 2 Outline of the MAX storage ring with its beamlines (Peter Röjsel).

Electrons from a "racetrack" microtron (Fig. 3) are injected into the storage ring at relatively low energy, about 100 MeV. In one of the straight sections there is a "kicker", a device for accelerating the electrons to operation energy. At the same time, the fields of all magnets have to be adjusted to keep the electrons on the right trajectory.

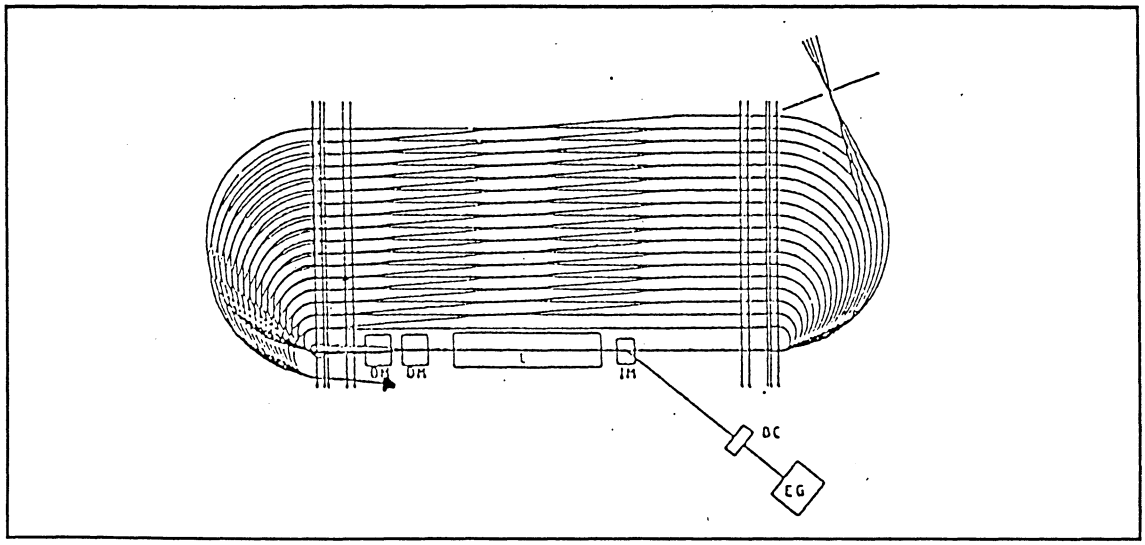

Fig. 3 The Racetrack Microtron used for injection of electrons at MAX [7].

In another straight section there is a radio frequency resonance cavity,

where the electrons pick up enough energy to compensate for the losses due to radiation. The cavity also divides the electron beam into "bunches", and this in fact gives the storage ring its characteristic time structure. In normal operation there are ten bunches of electrons evenly distributed around the ring.

The ring can also be operated in a single-bunch mode with only one bunch of electrons in the ring. This gives a lower repetition rate and a lower radiation flux, which is useful for certain experiments.

After injection and acceleration to operation energy, the current in the ring is typically 200 mA. A few electrons are lost in every revolution and the ring current will decay. At MAX, the present half-life of the stored electron current is about 45 minutes.

The MAX storage ring is used for nuclear physics experiments about 25% of the run-time. The ring then works as a pulse stretcher and an almost continuous beam of high-energy electrons can be extracted and directed to a target.

2.3 PROPERTIES OF THE RADIATION FROM MAX

We will list a few of the extremely useful properties of synchrotron radiation here and give examples based on parameters from MAX. A more thorough description of the radiation from MAX can be found in reference [7], from which a few of the figures in this section are taken.

Continuous wavelength spectrum

When the electron bunch is accelerated at the bending magnet, the electrons radiate energy in a wide spectral range. In fact, we obtain a very intense continuum, with photon energies ranging from the far infrared all the way up to the X-ray region. The typical spectrum from MAX is shown in Fig. 4.

Different synchrotron radiation facilities are often characterized by their characteristic or critical wavelength, λ_c, defined by (5). Approximately half of the radiated power falls below λ_c and half above. For the MAX storage ring the critical wavelength is 40 Å.

In the vacuum ultraviolet and X-ray regions, synchrotron radiation offers an intensity and a tunability generally difficult or impossible to obtain from any other source [2].

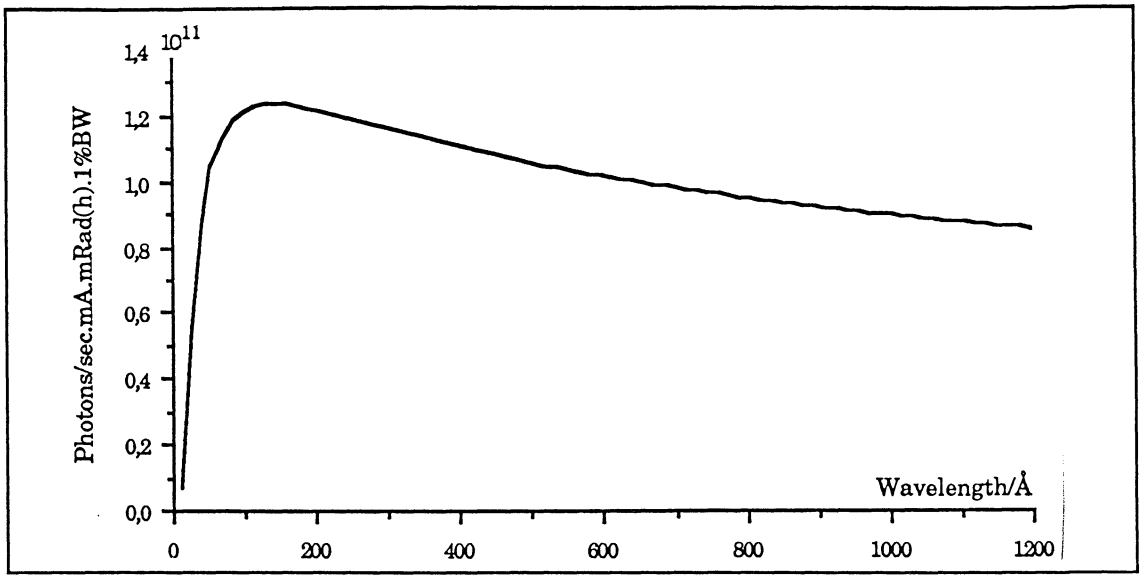

Fig. 4 Typical wavelength spectrum from MAX. The spectrum is calculated from equations (1) through (6) in Sect. 2.1, with parameters characteristic of beamline 52 at MAX.

The most obvious source in the infrared region is a black-body radiator. It is interesting to note, however, that the intensity per unit bandwidth in synchrotron radiation spectra decreases less rapidly with wavelength than that of a black-body radiator. For wavelengths in the region of 100-200 μm, a synchrotron radiation source can actually give a higher radiation flux than a black-body radiator. Of course, one must remember the greater physical convenience offered by a black-body source...

Polarization

The polarization of synchrotron radiation is well-defined, which is a very useful feature for a number of applications, e.g. for angle resolved photo-electron spectroscopy.

The radiation emitted in the plane of orbit is 100% polarized, with the electric field vector parallel to the orbital plane. Above or below this plane, the radiation is elliptically polarized, the degree of polarization depending on both viewing angle and wavelength. This is illustrated in Fig. 5.

In a real machine, there is a slight decrease in polarization even in the orbital plane, due to the finite size of the electron beam.

As mentioned before, the polarization properties can also be determined from (2), since the two terms inside the bracket of (2) are associated with the two components of polarization.

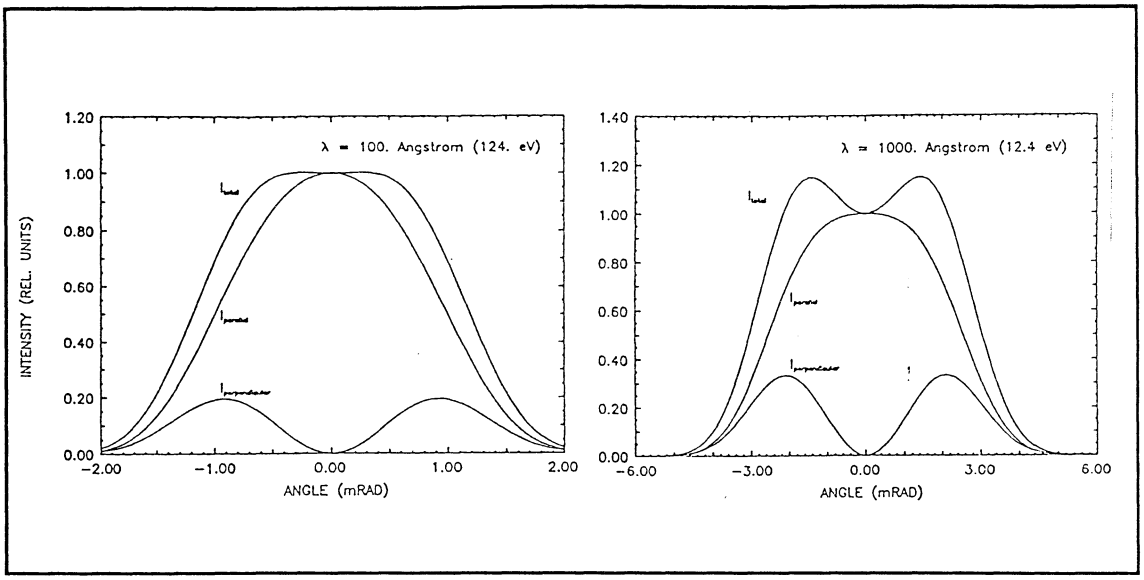

Fig. 5 The polarization components of synchrotron radiation from MAX as a function of vertical angle and wavelength [7]. Note that the angular divergence increases with wavelength.

Well collimated light and high brilliance

The highly relativistic electrons in a storage ring emit radiation in a narrow cone in the direction of motion, as shown in Fig. 1. The opening angle of the cone is approximately given by γ^{-1}. The angle of emission depends on the wavelength.

The spectral brilliance, or brightness, of a light source is defined as the photon flux per 0.1% bandwidth, unit source area and unit solid angle of emission, i.e. it is dependent upon both the directional properties of the radiation, and the size of the source as seen by the observer. In the case of a storage ring, the source is actually the electron beam itself. The cross-section of the electron beam can be very small; this property combined with the high collimation of the radiation gives the synchrotron radiation source a high brilliance over a wide spectral range.

Fast time structure

We have already mentioned that the appealingly fast time structure of the synchrotron radiation comes from the bunching of electrons in the resonance cavity of the ring. At MAX the pulses of radiation entering a beamline are as short as 80 ps and they are separated by about 10.8 ns, when all ten bunches are filled [8]. The intensity is very stable from bunch to bunch.

Maximum separation is obtained in single-bunch mode, where the period of revolution determines the repetition rate.

3. Beamline Design

3.1 THE FUNCTION OF A BEAMLINE

The most obvious function of the beamline is, of course, to connect a monochromator, if any, and the experimental set-up to the storage ring. It also provides a low-molecular conductance path to the experiment and a well defined source since the beam aperture closest to the ring often defines the source.

Matching of the source emittance

The beamline is designed in order to match the emittance of the radiation source to the acceptance of a monochromator or the experiment. Figure 1 shows one way to describe the general configuration of a synchrotron radiation experiment and the effect of the various components [2].

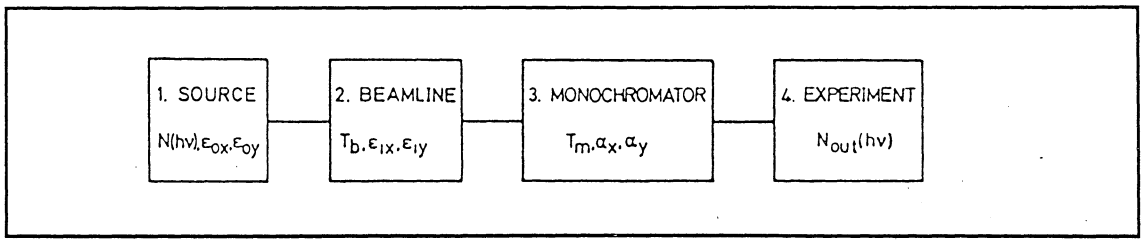

Fig. 1 A general configuration for a synchrotron radiation experiment [2].

The radiation source, i.e. the electron bunch, is characterized not only by the number of electrons and their energy, but also by its vertical and horizontal emittances (ε_{0x}, ε_{0y}). The emittance (ε) is defined as the product of the size (σ) of the source and the angular divergence (σ') of the emitted radiation, e.g. $\varepsilon_x = \sigma_x \sigma'_x$.

The optical elements (mirrors) in the beamline will transform the source emittance into the beamline emittance (ε_{1x}, ε_{1y}) and the radiation flux will be reduced by the beamline transmission coefficient T_b.

The definition of acceptance is analogous to that of emittance. The vertical and horizontal acceptances of the monochromator (α_x, α_y) are definied as the product of aperture size and acceptance angle.

To get maximum performance out of the monochromator and the highest possible flux at the experiment, it is absolutely essential that the

emittance of the beamline be matched to the monochromator acceptance. It is equally important that the beamline accept as much of the radiation from the source as possible.

Vacuum requirements

The storage ring works under high-vacuum conditions with pressures of 10^{-9} mbar or less. The pressure in the beamline has to be as low as that in the ring, or lower. The beamport at the storage ring is usually equipped with a fast-closing valve connected to a pressure trip to protect the storage ring. The generally small apertures and large volumes of mirror tanks help to slow down a sudden accidental pressure rise in the experimental set-up or in the monochromator long enough for the security interlock system to close the valve.

Physical constraints

The physical constraints of a synchrotron radiation beamline are considerable. First of all, the storage ring is surrounded by a radiation shield and thus the access to the area closest to the ring is limited. On the other hand it is desirable to place both the reflecting mirrors of the beamline and the monochromator itself as close to the source itself as possible. Otherwise the optical elements will be too large and the costs too high.

Second, there is often more than one beamline extending from the same bending magnet. Both beam pipes and mirror chambers must be pumped and the space available for pumps is limited.

It is not always easy to find enough space for the experimental set-up, let alone for the experimenters themselves...

3.2 OPTICAL ELEMENTS

In the vacuum ultraviolet (VUV) and soft X-ray regions, all known materials have very high optical absorption. Therefore reflecting optics (e. g. mirrors) are usually used to redirect, focus and diffract the radiation. For X-rays (< 30 nm), grazing-incidence techniques have to be used to obtain high enough reflectance from mirrors and gratings.

The coating material determines the spectral characteristics of a reflecting surface. The choice of coating depends upon application and wavelength region. At normal incidence in the VUV, gold, platinum,

osmium and ruthenium are common coating materials.

The roughness of the reflecting surface is of great importance in the VUV, where the dimensions of the surface irregularities are close to the wavelength of the light.

The first mirror in a beamline is designed to collect as much radiation as possible from the storage ring beam port. It also acts as a filter, absorbing or transmitting all of the hard X-rays, which otherwise could damage other components in the system (especially in the case of high-energy machines). The absorption of radiation energy is high so these mirrors operate at a high power load. Therefore it is important to provide adequate heat dissipation from the mirrors and to use mirror materials that will not suffer radiation damage by the X-rays.

Another hazard to optical surfaces is carbon contamination. Even in high-vacuum systems, the partial pressures of hydrogen, carbon monoxide and methane can be significant. These substances can undergo photo-induced chemical reactions to yield a thin layer of graphitic carbon on optical surfaces. The speed of this reaction is dependent upon both partial pressures of contaminants and radiation intensities. The vacuum systems of synchrotron radiation facilities must therefore be free of hydrocarbon sources, prohibiting the use of oil-diffusion pumps.

3.3 BEAMLINE 52 AT MAX

Figure 2 shows the beamline connected to beamport 52 of the MAX storage ring. The size of the radiation source is typically 0.3 mm (h) by 0.1 mm (v) and the angular divergence of the radiation 24 mrad (h) by 12 mrad (v) [9, 6].

A spherical mirror of radius 200 mm intercepts 20 mrad of the emitted radiation. The radius of curvature is 3170 mm. The mirror substrate is zerodur and it is coated with 1000 Å of gold, giving a reflectance of over 20% at 550 Å.

The mirror is located about 10 m from the electron beam and focusses the radiation to a spot located 2 m from the mirror.

A ray-tracing study of the beamline predicted a size of the focus spot of 0.5 mm (h) by 1 mm (v). The spot size is aberration limited, i.e the size of the source does not influence the spot size very much.

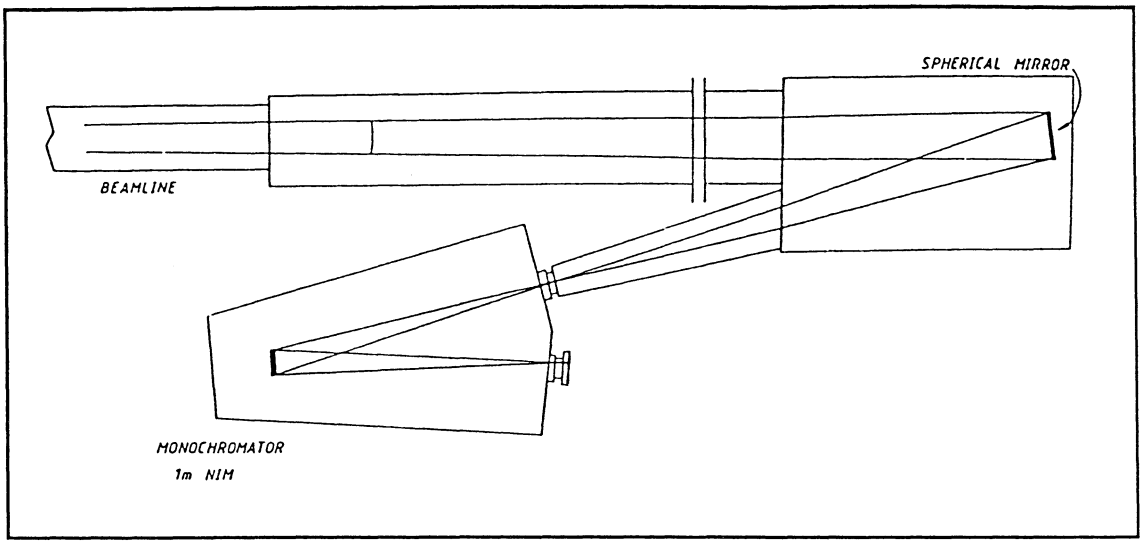

Fig. 2 An outline of beamline 52 at MAX-lab [6].

The intensity from the monochromator is limited by the size of the spot at the entrance slit. It is therefore essential that the monochromator be well aligned to the beamline, with the focus of the mirror right at the entrance slit. The mirror holder can be adjusted in all directions from outside of the vacuum chamber in order to achieve a good focus position.

4. Gratings and Monochromators

Optical spectroscopy is one of the most fundamental experimental methods in physics, consequently a high technical standard was achieved at an early stage.

Photons can be dispersed by a monochromator or spectrograph, either for use as an excitation source or for the study of radiation emitted by an excited sample. Over the years several different grating mounts and monochromator designs have been developed [2, 10].

As the use of synchrotron radiation has developed, more attention is being given to the development of grating technology and monochromator design. This results in more efficient and specific instruments which take advantage of the unique features of synchrotron radiation.

In this chapter we will discuss the fundamentals of the theory behind monochromator designs utilizing the concave grating.

4.1 CONCAVE GRATINGS

Why use concave gratings?

The use of plane diffraction gratings in monochromators involves at least three reflections. The first reflection is from the collimator, to make the incident light parallel and give all rays equal angle of incidence. The second is from the grating itself and the third reflection is from a focussing mirror which focusses the diffracted light onto the exit slit.

In the VUV, even the most suitable coating materials have a reflectance of less then 30%. It is clear that after three reflections the loss of intensity would be unacceptably high. A grating ruled in a concave surface combines all of these functions in one single surface thereby preserving as much of the initial flux as possible.

Grating efficiency and blaze

The grating efficiency, in a certain order and at a certain wavelength, is defined as the ratio of the output flux in this order to the total flux incident on the grating of this wavelength.

The intensity distribution into different spectral orders is largely a result

of the diffraction pattern of an individual ruling facet. Plane, symmetric ruling facets will diffract the maximum intensity into the zero order, which is not dispersed. By giving the ruling facet a shape like the one outlined in Fig. 1, the maximum of the intensity distribution can be shifted into one of the dispersed orders. A grating like this is said to be *blazed* for a certain wavelength, λ_{blaze}.

In Fig. 1, θ is called the blaze angle. This angle defines a wavelength for which there is a maximum of diffracted intensity. The angle coincides with the mirror-like reflection from the surface of a ruling facet. For this particular direction, the rule of reflection gives us $\alpha-\theta = \theta-\beta$, or

$$\theta = \frac{\alpha + \beta}{2}. \tag{1}$$

We will need the grating equation as derived later in this section:

$$m\,\lambda_{blaze} = d\,(\sin\alpha + \sin\beta). \tag{2}$$

By eliminating β from (1) and (2) we obtain the wavelength λ_{blaze} which fulfills the conditions outlined above.

$$m\,\lambda_{blaze} = 2\,d\,\sin\theta\,\cos(\alpha-\theta) \tag{3}$$

Manufacturers often specify the blaze wavelength at normal incidence, i.e. with $\alpha = 0$, reducing (3) to

$$m\,\lambda_{blaze} = d\,\sin 2\theta. \tag{4}$$

Even for near-normal incidence mounts, the factor $\cos(\alpha-\theta)$ in (3) is so close to unity, that (4) can be regarded as quite general.

From both (3) and (4) we can see, that if a grating is blazed at 500 Å, for example, in the first order, the blaze condition is also valid for 250 Å in second order, etc.

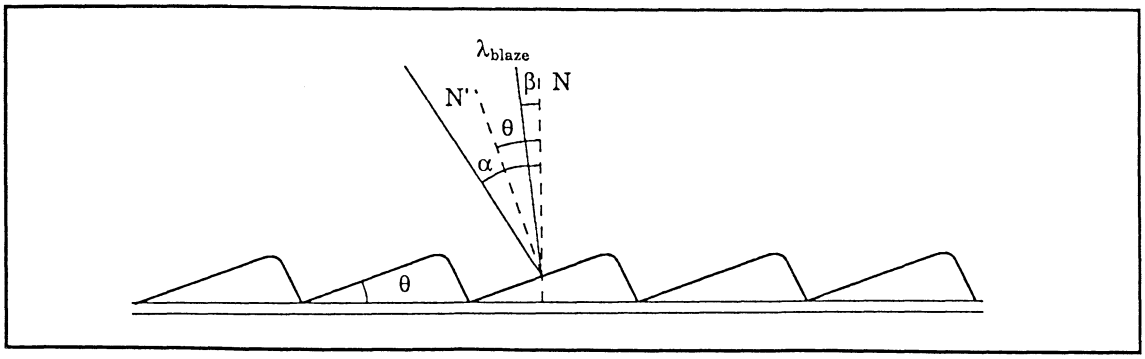

Fig. 1 The surface of a blazed grating. α and β are both positive, as written here.

Beutler's grating theory

Even a rather elementary geometrical study can show that good image quality is obtained by placing the concave grating and the slits along the so called Rowland circle. Rowland has made important contributions to the theory of imaging using concave gratings, although the fundamental theoretical formulation was completed by Beutler [11].

The short introduction to the theory presented here covers general points which are treated in more detail by Litzén [12] and Samson [10].

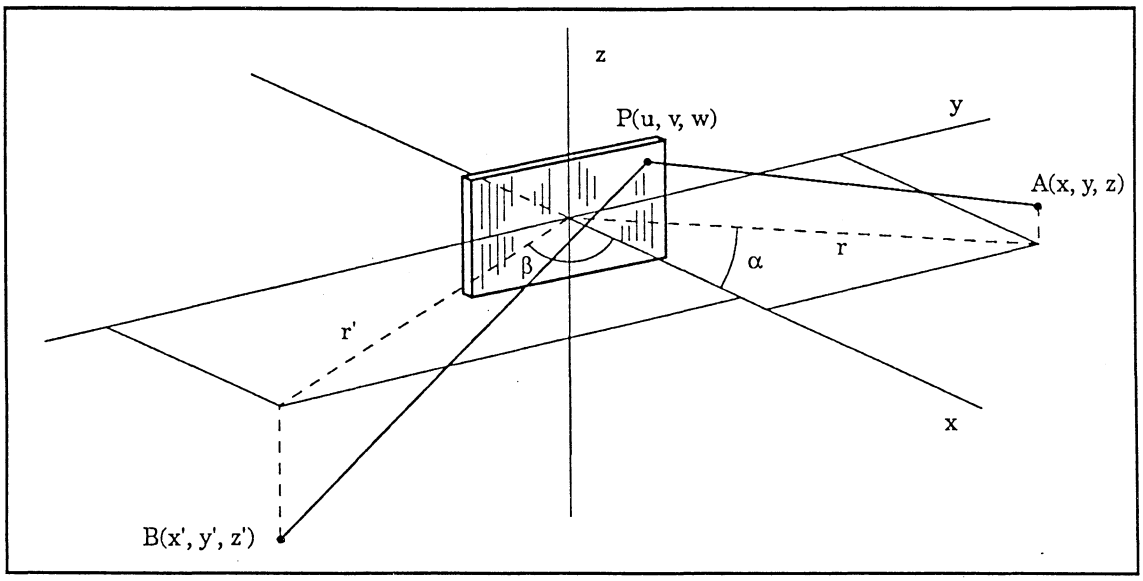

Fig. 2 Notation used for the description of grating theory.

Figure 2 shows a grating with arbitrary shape and curvature, where a ray of light from a point A(x,y,z) intersects the grating surface at a point P(u,v,w). The image of A is found at point B(x',y',z').

For the distances between points A, B and P we have

$$(AP)^2 = (x - u)^2 + (y - v)^2 + (z - w)^2, \tag{5}$$

$$(BP)^2 = (x' - u)^2 + (y' - v)^2 + (z' - w)^2. \tag{6}$$

We need to describe the shape of the grating surface in this coordinate system. We assume it is spherical with radius of curvature R, vertex on the x-axis and origin on the surface. All points on the surface can then be written as

$$(u - R)^2 + v^2 + w^2 = R^2 \tag{7}$$

The rulings of the grating are oriented in the z-direction. We intend to place the entrance and exit slits in the x-y plane, oriented parallel to the

rulings of the grating. It is therefore convenient to introduce cylindrical coordinates for points A and B:

$$x = r \cos \alpha \qquad y = r \sin \alpha \tag{8}$$

$$x' = r' \cos \beta \qquad y' = r' \sin \beta \tag{9}$$

Let us now consider the conditions that must be fulfilled to produce an image of point A at point B. We introduce a function F as the optical path length between points A and B:

$$F = AP + BP\,. \tag{10}$$

According to Fermat's principle, a light path is only possible if F has an extreme, i.e. if

$$\frac{\partial F}{\partial v} = \frac{\partial F}{\partial w} = 0. \tag{11}$$

We have an image of point A at B only if condition (11) is valid for all points on the grating surface, i.e. for all values of v and w. This is the condition for F = AP + BP to describe an image according to the law of reflection. It is equivalent to the requirement that all paths from A to B be of equal length. For a grating, however, this is not the whole truth. Only discrete strips of the grating (the ruling facets) reflect light and so other light paths are possible. Our condition must therefore be more specific – we require that all waves reaching B be in phase in order to form an image. To modify (10) to fulfill this condition, we include the light paths whose lengths differ only by an integral number of wavelengths, when v is changed with the ruling distance, d. Our new path-length function is now

$$F = AP + BP + \frac{m\lambda v}{d}\,. \tag{12}$$

If we use expressions (7), (8) and (9) in (5) and (6), respectively, we can write F as a function of r, r', α, β, z, z', v and w. To be able to handle this expression, we need to make a series expansion of the root expressions and organize all the terms according to their size. We choose to do this in nearly the same way as Beutler. We introduce a few new quantities:

$$AP = \sum F_i \tag{13}$$

$$BP = \sum F_i'\,. \tag{14}$$

Here we will only focus our attention on the first two terms in each of these expansions. They are

$$F_1 = r - v \sin \alpha \qquad (15\,a)$$

$$F_2 = \frac{1}{2} w^2 \left(\frac{\cos^2 \alpha}{r} - \frac{\cos \alpha}{R} \right) \sum_{i=0}^{\infty} \left(\frac{w \sin \alpha}{r} \right)^i \qquad (15\,b)$$

$$F_1' = r' - v \sin \beta \qquad (16\,a)$$

$$F_2' = \frac{1}{2} w^2 \left(\frac{\cos^2 \beta}{r'} - \frac{\cos \beta}{R} \right) \sum_{i=0}^{\infty} \left(\frac{w \sin \beta}{r'} \right)^i . \qquad (16\,b)$$

The image quality and focussing properties are described by this set of equations. Application of the condition in (11) at points on the grating surface allows us to evaluate the importance of aberrations to the image quality. The non-zero terms in (11) represent aberrations.

The Rowland circle

We start by examining a function $F^{(1)}$, ignoring all but the first terms, F_1 and F_1', and the "grating term" of (12).

$$F^{(1)} = r - v \sin \alpha + r' - v \sin \beta + m\lambda \frac{v}{d} \qquad (17)$$

According to Fermat's principle we will look for solutions that satisfy

$$\frac{\partial F}{\partial v} = 0 \qquad \frac{\partial F}{\partial w} = 0. \qquad (18)$$

The second condition is satisfied already, while the first gives us the condition

$$- \sin \alpha - \sin \beta + \frac{m\lambda}{d} = 0.$$

After rewriting we recognize this as the grating equation.

$$d (\sin \alpha + \sin \beta) = m\lambda \qquad (19)$$

This is the only condition we need to satisfy for plane gratings (for plane gratings, all other terms will vanish). For the concave-grating case, however, (19) only gives us the direction in which we can expect an image, but does not predict how far from the grating it will be found.

We would have a perfect focus at a point B if we could set the derivatives (18) to zero for all of the remaining terms in Beutler's expansion.

Unfortunately, this is not possible for a concave grating. Just as for concave mirrors, we will have both a horizontal and a vertical focus, a phenomenon known as astigmatism.

Our main concern is to obtain a good focus in the plane of dispersion, i.e we are mostly interested in the horizontal focus. This focus can be found using the second terms in Beutler's expansion, given by (15 b) and (16 b). We collect them in a function $F^{(2)}$:

$$F^{(2)} = \frac{1}{2} w^2 \left(\frac{\cos^2\alpha}{r} - \frac{\cos\alpha}{R} + \frac{\cos^2\beta}{r'} - \frac{\cos\beta}{R} \right) + \\ + \frac{1}{2} w^3 \left[\frac{\sin a}{r} \left(\frac{\cos^2\alpha}{r} - \frac{\cos\alpha}{R} \right) + \frac{\sin b}{r'} \left(\frac{\cos^2\beta}{r'} - \frac{\cos\beta}{R} \right) \right] + \ldots \quad (20)$$

If we take the first term of (20), and set its derivative with respect to v to zero, we obtain what is called the *Beutler focussing criterion:*

$$\frac{\cos^2\alpha}{r} - \frac{\cos\alpha}{R} + \frac{\cos^2\beta}{r'} - \frac{\cos\beta}{R} = 0. \quad (21)$$

One of the solutions to this equation can be written as

$$r = R\cos\alpha, \qquad r' = R\cos\beta. \quad (22)$$

These are the equations for a circle, with the radius $\frac{R}{2}$ and the points $A(r,\alpha)$ and $B(r',\beta)$ on the circle. This is the *Rowland circle.* Higher terms in (20) also vanish, along with other terms having the same α and β dependence. Other higher-order terms in the expansions do not, however, disappear. They represent aberrations, principally coma and astigmatism.

4.2 A FEW COMMON GRATING MOUNTS

Mounts along the Rowland circle

There are many different designs based upon the Rowland circle idea [2, 10, 12]. The principle is easy to implement in spectrographs, where the plate is placed along the circle. In instruments using both entrance and exit slits, at least one, or both, of the slits have to move along the circle. This will give rise to practical and mechanical problems, especially in the case of high-vacuum systems.

Monochromators working in grazing incidence are also frequently based upon the Rowland circle formulation.

The Seya-Namioka mount

There are also completely different solutions to the focussing problem. One of the most common is the Seya-Namioka mount [10]. This design is also based upon the Beutler focussing criterion (21), but now we are looking for a solution for the case in which the grating is rotated, but both slits are fixed with a constant opening angle, i.e. α is variable, but r, r' and $2\gamma = \alpha - \beta$ are constant at all wavelengths. Thus only a simple rotation is needed for a wavelength scan.

A closer study of (21) shows, that an approximate solution can be found for an opening angle ($2\gamma = \alpha - \beta$) of 70.5°. Higher-order terms will not be zero, however, so we can expect considerable aberrations and poor resolution. The use of curved slits can improve the situation slightly.

Simultaneous rotation and translation (MacPherson)

In most applications it is desirable to have fixed entrance and exit slits at all wavelengths. But if we simply rotate the grating, the slits will no longer be on the Rowland circle. It is possible to design a normal-incidence monochromator showing high resolution over a wide spectral range in spite of this. This is done by simultaneous rotation and translation of the grating along the slit bisector.

This is a design principle used by many commercial manufacturers, e.g. MacPherson and Minuteman. The monochromator on beamline 52 at MAX-lab is based upon the same principle and it will be described in detail in the next chapter.

5. Design of the Monochromator

During my spring at MAX-lab and beamline 52, most of our attention has been on the monochromator and its alignment. In this chapter we will therefore give a rather detailed description of the monochromator design and the algorithms used for its control. Measurements made to demonstrate resolution and wavelength calibration of the instrument will be presented in the next chapter, along with flux measurements using synchrotron radiation and a discussion of a few problems we encountered along the way.

5.1 BACKGROUND

Beamline 52 at MAX-lab is intended for experiments in the VUV region between 350 and 2000 Å. For this purpose a 1 m normal incidence monochromator has been designed [13, 21], i.e. an instrument using gratings with a 1 m radius of curvature and the light incident near the normal of the grating. In this case the angle between incoming and outgoing light is about 15°.

Both entrance and exit slits are fixed in position and thus the slits will not remain on the Rowland circle when the grating is rotated. To our great fortune, however, it is possible to find solutions to the the Beutler equations even off of the Rowland circle. If the entrance slit is displaced a distance d_1 outside the Rowland circle, the image of the entrance slit will be displaced approximately the same distance inside the circle (Fig. 1). Samson [10] calls this the "Off-Rowland Circle Mounting".

Since at least Beutler's first-order equations are satisfied, an instrument of this kind can give reasonable resolution over a large wavelength range provided that the grating can be translated along the slit bisector in order to maintain the focus at all wavelengths.

As mentioned in the previous chapter, this principle is used successfully by several commercial manufacturers, e.g. MacPherson and Minuteman [10]. In their instruments the movement of the grating is usually guided mechanically by a cam. Lewis [14] has shown how the focussing properties can be improved if the cam is accurately machined according to a complicated function derived from the focussing conditions.

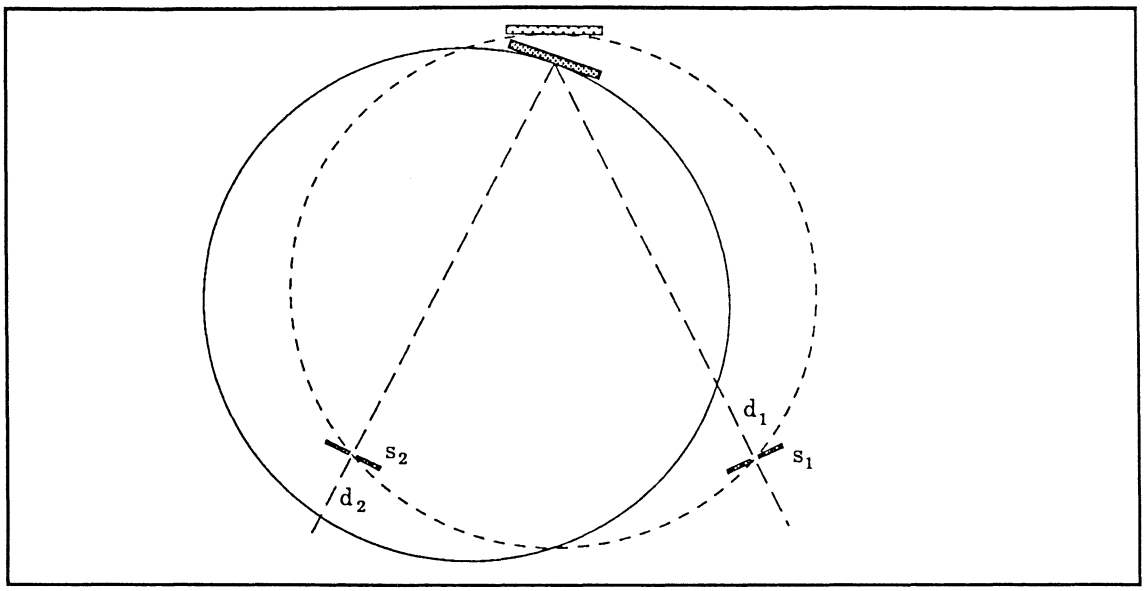

Fig. 1 The idea behind the off-Rowland circle mount. The grating is simultaneousely rotated and translated along the slit bisector.

The design used at beamline 52 presents a different solution. As showed in Fig. 2, the grating is simultaneously rotated and translated by means of two high-precision translator tables, controlled by a personal computer [13, 21]. The rotation and translation of the grating are calculated directly from the grating equation and the focussing condition for each wavelength.

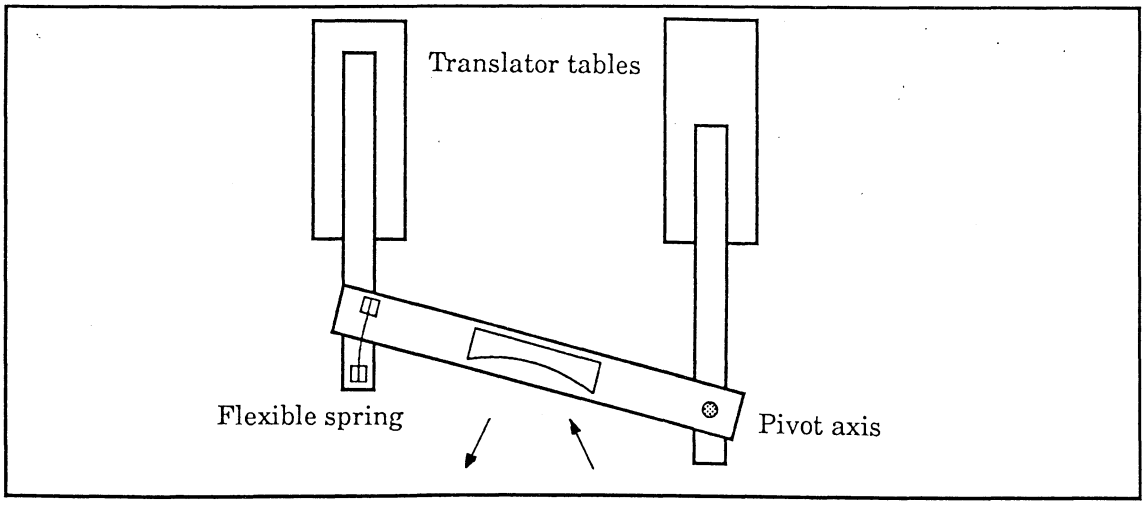

Fig. 2 An outline of the design of the monochromator at beamline 52. The grating is translated and rotated by means of two linear translator tables driven by stepping motors.

5.2 MECHANICAL CONSTRUCTION

The vacuum chamber and its support

The translator tables used for the grating movement are mounted on an 8 cm thick granite bench. The bilateral slits are also rigidly fixed to the same bench. The granite bench rests on three steel balls and can be translated as well as elevated for easy alignment with the rest of the beamline.

The monochromator is pumped by a grease-lubricated turbo-molecular pump, placed on top of the vacuum chamber. To avoid vibrations from the pump propagating to the grating support, the vacuum chamber is supported by a separate stand and connected to the slits and translator tables through flexible steel bellows.

Movement of the grating

The grating support is built to accept gratings in standard holders of the type which e. g. Minuteman uses in their instruments. These holders are easily fixed in the support and the position and orientation of the grating can be adjusted if needed.

Figure 2 shows how the grating support is held up by two circular steel rods, each rod fixed to its translator table through a steel bellows, which is not shown here. The grating can be both translated and rotated through the linear motion of the translator tables. The grating support is pivoted around an axis on top of the steel rod closest to the entrance slit. It is connected to the other steel rod with a flexible spring made of phosphor bronze. The fact that the grating is pivoted around an axis displaced from the grating vertex makes the grating movement asymmetrical and this results in a somewhat complicated set of equations for the calculations, as will be described in Sect. 5.3.

The translator tables and stepping motors are supplied as integral units by the French manufacturer "Micro Controle", model MT160. They have a resolution of 0.1 μm, i. e. each motor step corresponds to a table movement of 0.1 μm. This should not lead one to believe, however, that the accuracy and reproducibility are even close to that value. The latter quantities are specified to be in the range of 2 μm even under ideal conditions. In Sect. 6.3 we will consider what this means in terms of the overall positional accuracy.

5.3 ALGORITHMS FOR COMPUTER CONTROL

The two stepping motors are controlled by a personal computer via a motor interface and an i/o board. The control program is written in Turbo Pascal and offers the basic functions needed, such as scanning a wavelength range with a specified step width, moving the grating to a wavelength, moving each stepping motor separately for focussing adjustments, changing grating parameters, etc. The program can be ordered to wait for a ready-signal from other units in the experimental set-up before moving to the next wavelength in a scan.

The program automatically keeps track of the grating position and all current parameters are saved on a diskette every time the grating comes to a stop. At power-up, the stored parameters can be checked against counters on the stepping motors to ensure a consistent wavelength calibration.

In this section we will derive the algorithms used in the program to calculate the movement of the translator tables.

The pivot axis

As mentioned before, the grating is pivoted about an axis on top of the steel rod closest to the entrance slit (Fig. 2). We will start by expressing the grating position in terms of the parameters ξ and δ, where ξ represents the position of the pivot point along the direction of movement of the steel rod and δ is the pivot angle of the grating support. Both ξ and δ are defined to be zero when the monochromator is focussed and in the zero-order position.

In Fig. 3 we have illustrated the grating in two positions; in "A", with zero-order light in focus, and in "B", with a wavelength λ in focus. Some of the angles and distances are largely exaggerated. Looking at the zero-order position ("A"), we now define a few parameters characteristic of the grating and the grating support:

R = radius of curvature for the grating used,

p = the distance from the pivot point to the grating vertex in the direction perpendicular to the steel rod,

t = the distance from the pivot point to the grating vertex in the direction parallel to the steel rod,

α_0 = the angle between the grating normal and the entrance slit at zero-order.

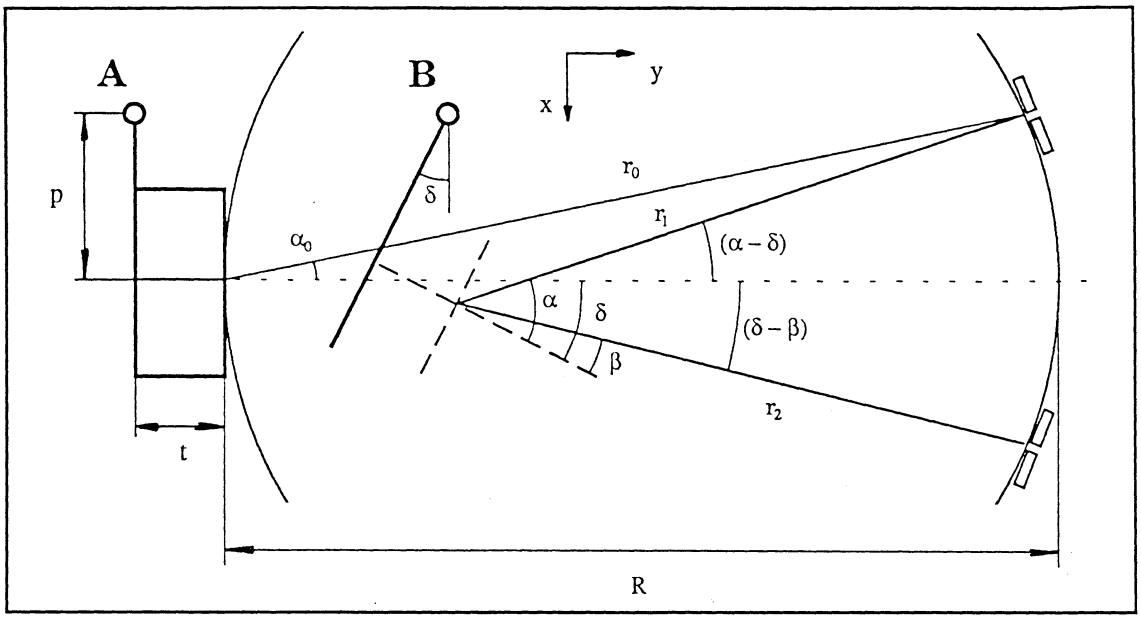

Fig. 3 The geometry of the grating movement.

From the figure we can see immediately that

$$r_0 = R \cos \alpha_0. \tag{1}$$

We will now derive a number of relations describing the geometry in Fig. 3 ("B") when a certain wavelength, λ, is focussed on the exit slit. We start out with the vertical and horizontal projections of r_0 and express them in terms of r_1 and r_2. This operation gives us four linearly independent equations. We begin with r_1 and use (1) to eliminate r_0:

(y) $$r_0 \cos \alpha_0 = r_1 \cos(\alpha-\delta) + t \cos \delta + \sin \delta \left(\frac{p}{\cos \delta} - p \right) - p \tan \delta + \xi - t$$

$$r_1 \cos(\alpha-\delta) = R \cos^2 \alpha_0 - t \cos \delta + p \sin \delta - \xi + t \tag{2}$$

(x) $$r_0 \sin \alpha_0 = r_1 \sin(\alpha-\delta) - t \sin \delta + \cos \delta \left(\frac{p}{\cos \delta} - p \right)$$

$$r_1 \sin(\alpha-\delta) = R \sin \alpha_0 \cos \alpha_0 + t \sin \delta - p\,(1-\cos \delta) \tag{3}$$

The same procedure applied to r_2 gives us the other two:

(y) $$r_0 \cos \alpha_0 = r_2 \cos(\delta-\beta) + t \cos \delta + \sin \delta \left(\frac{p}{\cos \delta} - p \right) - p \tan \delta + \xi - t$$

$$r_2 \cos(\delta-\beta) = R \cos^2 \alpha_0 - t \cos \delta + p \sin \delta - \xi + t \tag{4}$$

(x) $$r_0 \sin\alpha_0 = r_2 \sin(\delta-\beta) + t \sin\delta - \cos\delta\left(\frac{p}{\cos\delta} - p\right)$$

$$r_2 \sin(\delta-\beta) = R \sin\alpha_0 \cos\alpha_0 - t \sin\delta + p\,(1-\cos\delta) \tag{5}$$

We now add the grating equation (3.19) and Beutler's focussing criterion (3.21) to this system of equations:

$$\sin\alpha + \sin\beta = \frac{m\lambda}{d} \tag{6}$$

$$\frac{\cos^2\alpha}{r_1} - \frac{\cos\alpha}{R} + \frac{\cos^2\beta}{r_2} - \frac{\cos\beta}{R} = 0 \tag{7}$$

At this point we have six linearly independent equations, (2) through (7), and the same number of unknown quantities, namely α, β, r_1, r_2, δ and ξ. We consider the wavelength λ to be known and seek δ and ξ. From (2) through (5) we solve α, β, r_1 and r_2.

We divide (3) by (2) and get

$$\tan(\alpha-\delta) = \frac{R \sin\alpha_0 \cos\alpha_0 + t \sin\delta - p\,(1-\cos\delta)}{R \cos^2\alpha_0 - t \cos\delta + p \sin\delta - \xi + t}$$

$$\alpha = \delta + \arctan\left(\frac{R \sin\alpha_0 \cos\alpha_0 + t \sin\delta - p\,(1-\cos\delta)}{R \cos^2\alpha_0 - t \cos\delta + p \sin\delta - \xi + t}\right) \tag{8}$$

In the same way we divide (5) by (4):

$$\tan(\delta-\beta) = \frac{R \sin\alpha_0 \cos\alpha_0 - t \sin\delta + p\,(1-\cos\delta)}{R \cos^2\alpha_0 - t \cos\delta + p \sin\delta - \xi + t}$$

$$\beta = \delta - \arctan\left(\frac{R \sin\alpha_0 \cos\alpha_0 - t \sin\delta + p\,(1-\cos\delta)}{R \cos^2\alpha_0 - t \cos\delta + p \sin\delta - \xi + t}\right) \tag{9}$$

From (2) and (4) we solve for r_1 and r_2, respectively.

$$r_1 = \frac{R \cos^2\alpha_0 - t \cos\delta + p \sin\delta + t - \xi}{\cos(\alpha-\delta)} \tag{10}$$

$$r_2 = \frac{R \cos^2\alpha_0 - t \cos\delta + p \sin\delta + t - \xi}{\cos(\delta-\beta)} \tag{11}$$

To simplify these expressions we introduce a new function,

$$g(\delta) = R \cos^2\alpha_0 - t \cos\delta + p \sin\delta + t \tag{12}$$

and rewrite expressions (10) and (11) as

$$r_1 = \frac{g(\delta) - \xi}{\cos(\alpha - \delta)} \tag{13}$$

$$r_2 = \frac{g(\delta) - \xi}{\cos(\delta - \beta)} . \tag{14}$$

In (7), r_1 and r_2 are substituted by (13) and (14) and we solve for ξ.

$$\xi = f(\alpha,\beta,\delta) = g(\delta) - \frac{R\left[\cos^2\alpha \cos(\alpha - \delta) + \cos^2\beta \cos(\delta - \beta)\right]}{\cos\alpha + \cos\beta} \tag{15}$$

This is an implicit expression for ξ, since both α and β, given by (8) and (9), are functions of ξ. Now when we think about it – we have no explicit expression for δ, either.

The whole system thus has to be solved iteratively and we need initial values for α, β and δ. The easiest way to get these is to study the symmetric case (Fig. 4), where the grating vertex is moving along the slit bisector.

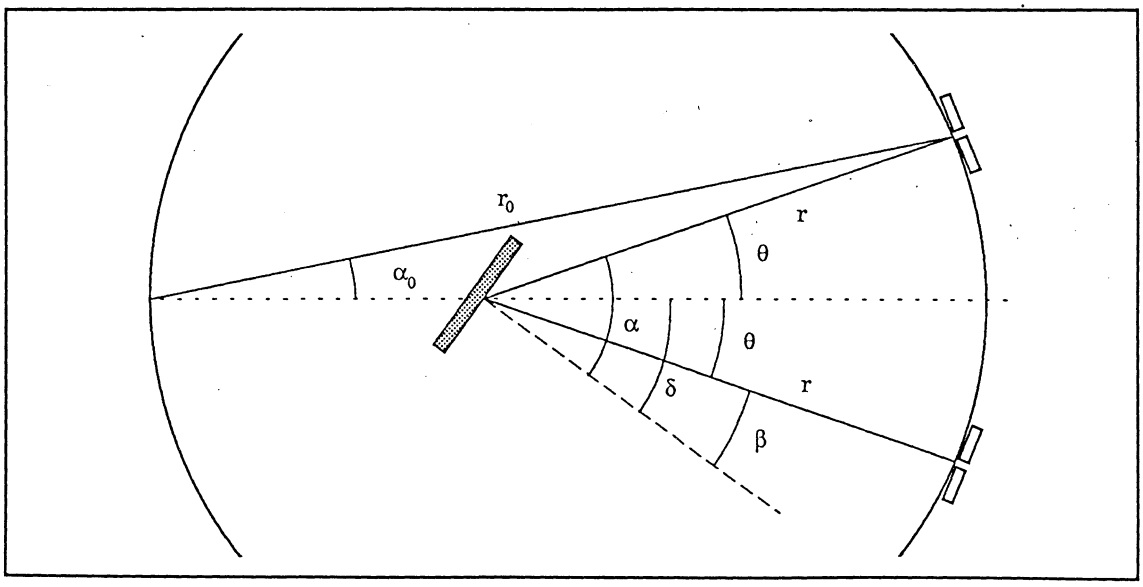

Fig. 4 The geometry of the symmetric case, used to obtain initial values for the iteration in the control program.

In this geometry we have

$$\theta = \frac{\alpha - \beta}{2} \tag{16}$$

$$\delta = \frac{\alpha + \beta}{2} . \tag{17}$$

Naturally, both the grating equation and the focussing criterion are still valid and we write

$$\sin\alpha + \sin\beta = \frac{m\lambda}{d} \tag{18}$$

$$\frac{\cos^2\alpha}{r} - \frac{\cos\alpha}{R} + \frac{\cos^2\beta}{r} - \frac{\cos\beta}{R} = 0 \ . \tag{19}$$

If we solve for α and β from (16) and (17) and apply them to (18), we get the expressions we will use to calculate initial values for the iteration.

$$\sin\delta = \frac{m\lambda}{2d\cos\theta} \tag{20}$$

$$\alpha = \theta + \delta \tag{21}$$

$$\beta = \delta - \theta \tag{22}$$

Here $\theta = \alpha_0$ can be used as a good enough approximation of θ.

Now we have all the tools we need. In the control program the calculations are organized in the following manner:

1. For the desired wavelength, $\lambda_{desired}$, initial values for α, β and δ are calculated using equations (20), (21) and (22).

2. Equation (15) is used to calculate $\xi = f(\alpha,\beta,\delta)$.

3. Equations (8) and (9) are used to calculate α and β.

4. The grating equation (6) now gives us the wavelength, $\lambda_{calculated}$, calculated with the latest values of ξ and δ.

5. The difference between the desired wavelength and the wavelength obtained so far is calculated as
   $$\Delta\lambda = \lambda_{desired} - \lambda_{calculated}.$$

6. We now want to translate the wavelength correction, $\Delta\lambda$, to a correction of δ, which we call $\Delta\delta$. Since the wavelength is a monotonic function of the pivot angle, δ, we can write
   $$\frac{\Delta\delta}{\delta} = \frac{\Delta\lambda}{\lambda}$$
   or
   $$\Delta\delta = \Delta\lambda\frac{\delta}{\lambda} \ .$$

7. The improved calculated value for δ is
$$\delta_{i+1} = \delta_i + \Delta\delta.$$

8. If the $\Delta\lambda$ we have so far is less than the maximum tolerable discrepancy set in the program (0.01 Å), the program moves on to "9". Otherwise it jumps back to "2" for another iteration.

9. Equation (15) is used again to calculate the final value for ξ.

10. Ready!

A remaining wavelength discrepancy of less than 0.01 Å is reached in only 3 or 4 iterations.

The flexible spring

So far we have calculated the position for one of the steel rods (ξ) and the grating pivot angle (δ). With the help of these two quantities we now have to calculate the corresponding position of the other steel rod. To do this we need a model that describes the bending of the flexible spring connecting the grating support to the steel rod.

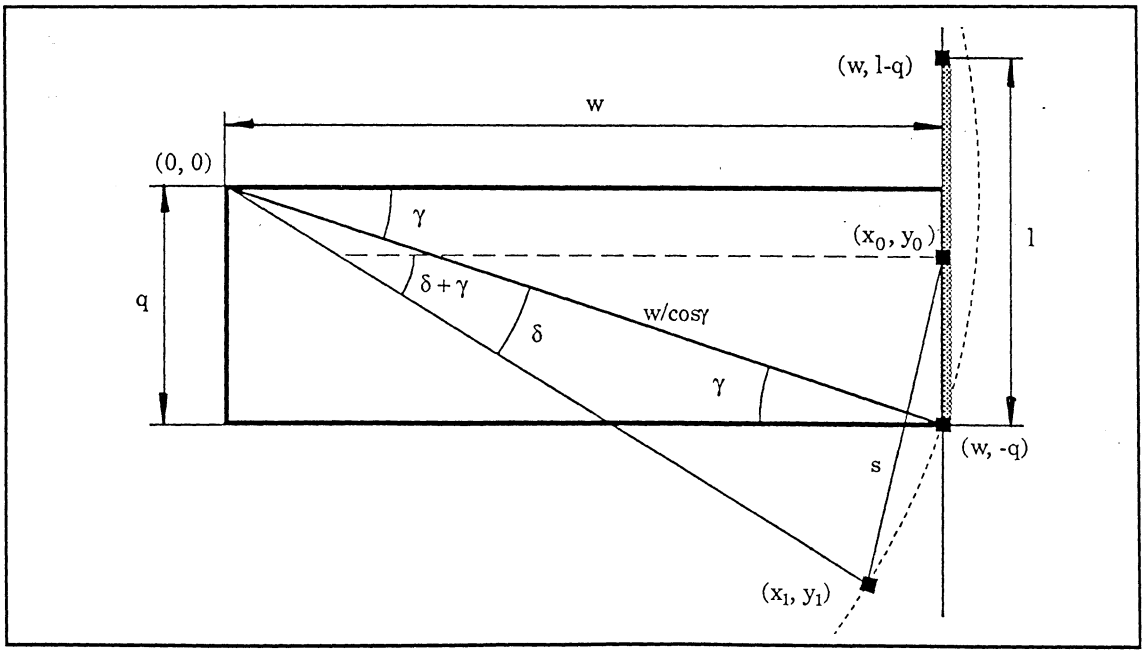

Fig. 5 The geometry used to model the flexible spring.

For the calculation in the program we assume that the spring is bending along the arc of a circle. The geometry is outlined in Fig. 5, where the pivot axis of the grating support is placed at the origin. The parameters q and w are defined (with $\delta = 0$) as the distances parallel and perpendicular to the translator movement between the pivot point and the spring end

attached to the grating support.

To obtain the correct pivot angle, δ, at the desired wavelength, the spring end on the grating support must be at point (x_1, y_1). The other end of the spring will then be at point (x_0, y_0). Because the linear motion of the translator table is parallel to the y-axis, x_0 equalls w at all times. We must calculate y_0 in order to put the translator table in the correct position. From Fig. 5 we have the following relations:

$$\gamma = \arctan\left(\frac{q}{w}\right) \tag{23}$$

$$x_1 = \frac{w \cos(\gamma + \delta)}{\cos\gamma} \tag{24}$$

$$y_1 = -\frac{w \sin(\gamma + \delta)}{\cos\gamma} \tag{25}$$

$$(x_0 - x_1)^2 + (y_0 - y_1)^2 = s^2 \tag{26}$$

$$x_0 = w \tag{27}$$

The flexible spring bends to form a circular sector with an arc of length l. A cursory look at Fig. 5 might give the impression that the angle of the arc is $\delta+\gamma$. However, the spring end is fixed in an angle displaced with γ from the outlined circle. The angle in question is therefore reduced to δ. This results in the following relationship between s and l:

$$s = \frac{2\,l \sin\left(\frac{\delta+\gamma}{2}\right)}{\delta+\gamma} \tag{28}$$

We now substitute (24) and (25) into (26) and solve for y_0:

$$y_0 = \sqrt{s^2 - w^2\left(1 - \frac{\cos(\delta+\gamma)}{\cos\gamma}\right)^2} - \frac{w \sin(\delta+\gamma)}{\cos\gamma} \tag{29}$$

The spring end fixed on the steel rod should be translated from (w, l–q) to (w, y_0). We call the position of this steel rod ψ, and just as for ξ we set $\psi = 0$ when the monochromator is in focus and at zero-order. Summing everything up and adding the movement of the pivot point, we get

$$\psi = l - q - y_0 + \xi. \tag{30}$$

6. Performance of the Monochromator

Now that we are familiar with the design of the monochromator at beamline 52, it is time to have a closer look at its performance.

First we will present the measurements which were made to determine the resolution and wavelength calibration of the instrument. After that we will have a look at the measured photon flux using the synchrotron radiation from the MAX storage ring. Finally, we will briefly discuss a few of the problems we have encountered along the way.

6.1 RESOLUTION AND WAVELENGTH CALIBRATION

The light source

The continuous nature of the synchrotron spectrum makes it necessary to use some kind of discrete line source for resolution and calibration measurements. The monochromator may be disconnected from the beamline mirror tank. A valve in the pipe down stream from the mirror tank can be closed and a blank flange in the connecting section on the monochromator can be replaced with a gas inlet and a hollow cathode just in front of the entrance slit. This provides us with a source of discrete lines characteristic of the ions produced in the hollow cathode.

A bottle filled with gas is connected to the gas inlet. The gases used are argon, krypton and helium. The hollow cathode is supplied with high voltage from a power supply via a load resistance. A discharge current of 60 mA is obtained with a voltage of about 1 kV, dependent on gas pressure.

The low gas conductance through the entrance slit results in a monochromator pressure of less than 10^{-6} mbar, despite the relatively high gas pressure in the connecting section.

The detector

After the exit slit the light is detected with an Al_2O_3 diode. As is apparent in Fig. 6 it is not much of a diode, but rather an aluminium slab with a very well defined oxide layer on the surface [10].

Photons incident on the surface release electrons from the metal through

the photo-electric effect. In front of the slab there is a collector ring biased to a positive voltage of about 150 V. The collector attracts the electrons and prevents them from falling back onto the aluminium surface. The current from the slab is measured with a sensitive electrometer. The diode is calibrated by NIST (National Institute of Standards and Technology) and there is a calibration curve of the quantum efficiency so the measured current can be translated into photon flux for each wavelength.

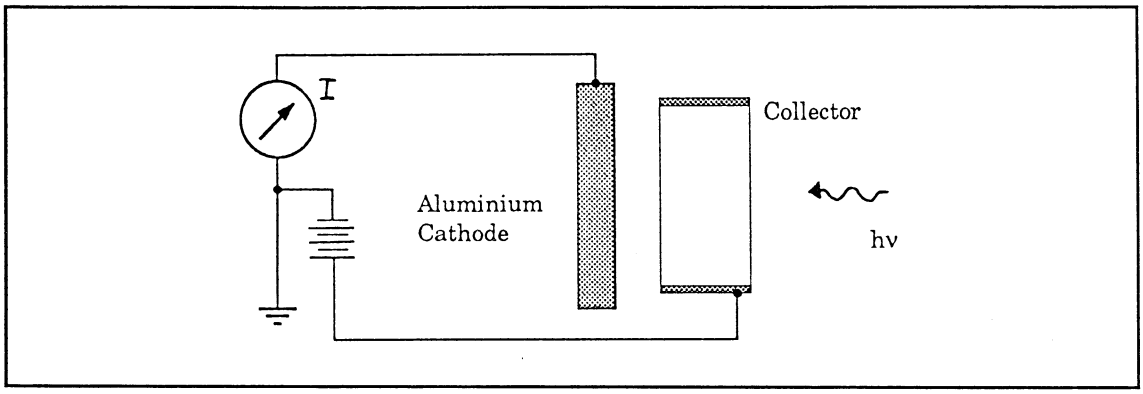

Fig. 1 The aluminium (Al_2O_3) photodiode used for absolute flux measurements.

Expected resolution

Because of the finite size of the light spot at the entrance slit the resolution in our set-up is dependent on the slit width alone. It is therefore of great interest to us to know just how dispersed the light is at the exit slit. With this in mind we write the dispersion relation which is simple to derive from the grating equation [10]:

$$\frac{d\lambda}{dl} = \frac{d \cos \beta}{mR} , \tag{31}$$

where dl is a small distance along the Rowland circle at the exit slit. The quantity $d\lambda/dl$ is called the *plate factor* and is the reciprocal of the *linear dispersion,* $dl/d\lambda$. In our construction the exit slit will be displaced from the Rowland circle, but the displacement is very small compared to the grating radius and we can therefore consider the relation to be a very close approximation even in our case.

Our monochromator is at present equipped with a 1200 lines/mm grating and in first order, i.e. with m=1, equation (31) yields

$$\frac{d\lambda}{dl} \approx 8.3 \text{ Å/mm}. \tag{32}$$

The best resolution we can expect is obtained simply by multiplying this

value by the slit width. In practice the resolution is determined by how well focussed the instrument is.

To focus the monochromator properly, one has to first of all find the zero-order position. In this position the position parameters in the program for both translator tables are set to zero. The zero-order peak is scanned with narrow slits and the width of the peak is measured. Then both translator tables are moved forward or backward a small distance and the zero-order peak is scanned again. The procedure is repeated in a systematic way until the best focus is found. This could indeed be a rather tedious work, but it is easier if a coarse focus has already been found using Focault's knife-edge test at atmospheric pressure with a simple spectral lamp as light source and a human eye at the exit slit [10, 12].

Results from measurements

A representative example of the results is shown in Table 1. Resolution measurements made of a He I line at 584.4 Å are tabulated for different slit openings. The resolution in both first and second orders are stated, as well as the resolution of the zero-order peak.

The results agree well with expectations. The ratio between the intensities in first and second order is found to be 8:1 at 584.4 Å.

Table 1 Resolution of the monochromator (FWHM). Measurements made of the He I line at 584.4 Å.

	Resolution FWHM (Å)		
Slit width (μm)	Zero-order	First order	Second order
100	1.0	1.0	0.5
150	1.1	1.1	0.55
200	1.3	1.4	0.7
250	1.6	1.6	0.8
300	2.0	2.0	1.0
400	2.5	2.5	1.3
500	4.0	4.0	2.1

The wavelength calibration was checked on a number of lines using different gases. Table 2 shows a comparison between measured and tabulated wavelengths for a few of these lines. It should be noted that we have had problems with reproducibility of these results. In extreme cases the peaks can be shifted up to 1 Å in position. These problems will be

discussed in Sect. 6.3 of this chapter. The results in Table 2 are from long uninterrupted scans with each gas.

With the reproducibility problems still in mind, the calibration looks reasonably good for most of the lines. In the case where remaining discrepancies are consistent and depend on construction parameters, either the parameters can be adjusted, or a correction function can easily be incorporated in the control program.

Table 2 A comparison between tabulated and measured wavelengths for a few different spectral lines.

Tabulated wavelength (Å)		Measured wavelength (Å)	
0	(Kr)	0	Position reset...
919.781	(Ar II)	919.7	
932.053	(Ar II)	929.9	
1066.659	(Ar I)	1066.5	
1839.562	(Ar II)	1839.5	919.781 Å in 2nd order
916.703	(N II)	916.8	
1085.701	(N II)	1085.75	
1134.981	(N I)	1135.0	
1200.223	(N I)	1200.4	
1037.0	(C II)	1036.9	Contamination?
584.334	(He I)	584.5	

6.2 MEASUREMENTS WITH LIGHT FROM THE MAX STORAGE RING

The performance of the monochromator using synchrotron radiation has been studied during several stages of my work at the beamline. This has been done with several different detectors in front of the exit slit, namely a channeltron, a NIST-calibrated GaAs photodiode and, finally, with the aluminium diode discussed in Sect. 6.1 (Fig. 1).

The channeltron was only used during the early phase of testing, when we were interested in whether we had any light through the monochromator. The channeltron is characterized by a very high quantum efficiency for photons in the VUV.

Then the calibrated GaAs photodiode was used, equipped with a 1.5 mm diameter aperture in an aluminium mask. The photodiode was fixed on a x-y-z manipulator allowing the shape and angular distribution of the light

fan from the exit slit to be measured. This is important to us, since we use a glass capillary in the experimental set-up to guide the radiation into the experimental chamber from a point approximately 7 cm away from the exit slit. The well-known spectral characteristics of the photodiode also enabled us to make measurements of the photon flux.

The aluminium photodiode was very convenient to use for our final adjustments and absolute photon flux measurements, since its large area is capable of accepting all of the radiation from the monochromator.

Asymmetric line shape

During alignment and focussing procedures we noted an asymmetry in the line shape, which seemed to be very sensitive to the alignment of the monochromator to the beamline and to the grating focus. In some positions, it looked more like *two* very close peaks... It was not very difficult, however, to minimize the asymmetry to a degree where it only appears as a very slight broadening of the line at one side near its base, and we therefore feel confident that it will not affect experiments.

Looking back at measurements with the hollow-cathode lamp we could see a similar tendency. At least in that case it seems reasonable to believe that it is an aberration effect of some kind.

Results from measurements

The aluminium photodiode (Fig. 1) was used for absolute photon flux measurements. The results are found in Fig. 2 and in Table 3.

According to a ray-tracing study (Sect. 3.3), the spherical mirror in the beamline focusses the radiation to a spot with a horizontal width of about 0.5 mm at the entrance slit. As long as the width of the entrance slit is smaller than the size of the focus spot, the slit width will limit the number of photons incident on the grating surface and the photon flux per unit wavelength will thus depend on the slit width; if the slit width is increased, the photon flux will also increase. The present measurements were made with a slit width of 0.2 mm.

In Fig. 2 the measured photon flux is compared to a calculated spectrum. This spectrum was calculated using equations (2.1) through (2.6) in Sect. 2.1, with parameters characteristic of beamline 52. This yields the absolute photon flux entering the beamport of the beamline. The spectrum was then convoluted with two successive reflections from gold surfaces, representing the spherical mirror in the beamline and the grating. The

efficiency of the grating, the acceptance of the monochromator and contributions from higher orders were not included. The reflectance data for gold is from reference [15].

By scaling down the calculated spectrum by a factor of 45, the peak at 560 Å in the calculated spectrum can be directly compared to the peak in the measured spectrum. For the wavelength of 560 Å the factor of 45 can be interpreted as the effect of the parameters not accounted for, e.g. grating efficiency, acceptance of the monochromator, etc.

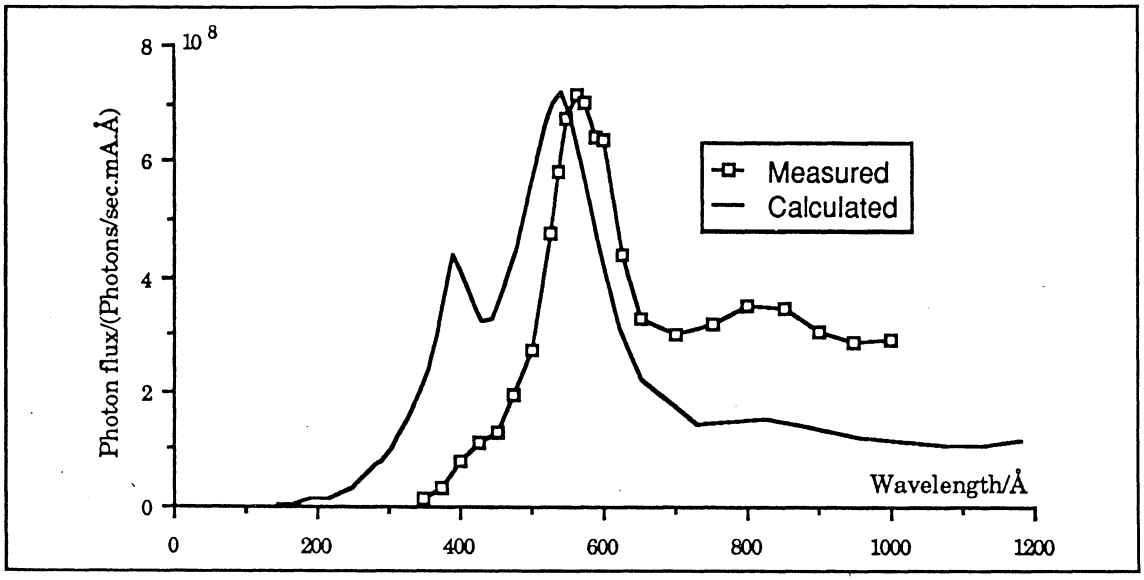

Fig. 2 Comparison between measured and calculated photon flux (see text). The slit width is 0.2 mm. The calculated spectrum has been scaled down by a factor of 45 for comparison to the measured spectrum.

Table 3 Results of absolute flux measurements using the aluminium photodiode. The flux is given per mA ring current and Å. The slit width was 200 μm.

Wavelength (Å)	Diode current (nA)	Photon flux per mA ring current (photons/sec/mA/Å)
400	0.15	0.8×10^8
450	0.24	1.3×10^8
500	0.55	2.8×10^8
550	1.55	6.8×10^8
600	1.42	6.4×10^8
650	0.92	3.3×10^8
700	0.83	3.0×10^8
700	0.83	3.0×10^8
800	0.74	3.5×10^8
900	0.48	3.1×10^8
1000	0.28	2.9×10^8

The intensity of the measured spectrum is clearly shifted towards higher wavelengths compared to the calculated spectrum, since the grating is blazed at 800 Å. It is hard to say if the grating efficiency alone is responsible for the apparent shift of the peak at 560 Å. There might also have been a slight offset in the calibration of the monochromator at the time of the measurement. It is also interesting to note, that for some unknown reason the smaller peak at 400 Å in the calculated spectrum (originating from the reflectance of gold) is not clearly recognized in the measured spectrum.

Measurements using the other detectors show similar results when the spectral sensitivities of the different detectors are compensated for.

6.3 PROBLEMS ENCOUNTERED

Slits

We have had problems with the slits getting stuck once in a while. Since then the slits have been redesigned to reduce the friction experienced by the moving parts. They now seem to work rather well, but we will keep looking for a better solution.

Wavelength shifts

During wavelength calibration and focussing, we have noticed that peaks can shift up to ±1 Å between scans.

After having eliminated other possibilities we arrived at the conclusion that it was due to low accuracy and reproducibility of the translator tables moving the grating. In order to study the problem we spent a week trying to build up a Michelson interferometer behind the monochromator chamber, with the moving mirror on one of the translator tables. This attempt failed, because the interferometer was built on a separate stand and vibrations in the monochromator stand made it impossible to count fringes.

In the specifications [16] the translator tables are said to have an accuracy of within 2 μm. We have made calculations based upon the monochromator geometry and grating parameters, which show that this would correspond to a wavelength inaccuracy in the range of 0.2 Å in a first-order approximation independent of wavelength. The inaccuracy we have seen exceeds this calculated value.

We have compared the actual load on the translator tables with the specified load capacity [16] and found that the actual horizontal load is greater than the specified capacity. The vertical load is within specification limits, but the torque exerted by the vertical and horizontal loads in combination is considerable and its effect hard to estimate from the information given in the specifications.

It is hard to say how much of the observed inaccuracy that can be blamed on the heavy load, but I find it probable that the situation would at least improve if the load was reduced.

The horizontal load is caused by the air pressure on the end of the bellows on the vacuum tank. The most effective measure would be to balance this force with heavy counterweights, strong springs, or – preferably – a combination of both.

The vertical load is caused by the weight of the grating and the massive steel rods supporting it, as well as the torque exerted by these heavy elements and the air pressure in combination. The vertical load can be reduced if the massive steel rods are exchanged with steel tubes of the same diameter and counterweights placed on the other side of the tables can compensate for the exerted torque. The material of the steel tubes should be thick enough to preserve the rigidity of the grating support.

7. The Experiment

During my time at the lab I had hoped to see at least the first results of the proposed experiments. Unfortunatelly the project has been delayed, mostly due to repeated problems with the mass spectrometer used for ion detection.

When this is written we hope to have everything working by the beginning of August 1990.

7.1 THE PROPOSED EXPERIMENT

The gas-phase experiments proposed by Elisabeth Källne's group in Stockholm involve the study of the inner-valence region of molecules such as NO, O_2, H_2, CO_2 and CO. The energies of interest all lie in the range covered by the normal incidence monochromator described in this work, i.e. 350-2000 Å.

The inner-valence region of these gases has been studied exstensively by a number of different groups [17, 18]. Photoelectron spectroscopy has revealed information about electron energy levels and ionization cross sections.

With the experimental set-up at beamline 52 we intend to study the dissociation products of these molecules as a function of photon energy. With a quadrupole mass spectrometer both positive and negative ions can be detected and absolute dissociation and ionization cross sections can be determined.

7.2 THE EXPERIMENTAL SET-UP

Differential pumping

Since the experiments are performed on gases, differential pumping is needed to allow a relatively high pressure in the interaction region, without affecting the pressure in the monochromator and in the beamline too much.

Figure 1 shows the experimental set-up connected to the monochromator. A 66 cm long glass capillary with an inner diameter of 3 mm is used as a

light guide, leading the light from a point about 7 cm outside the exit slit, through a pumped middle section and into the experimental chamber. The position of the capillary can be adjusted from the outside by means of two linear feed-throughs mounted on the middle section.

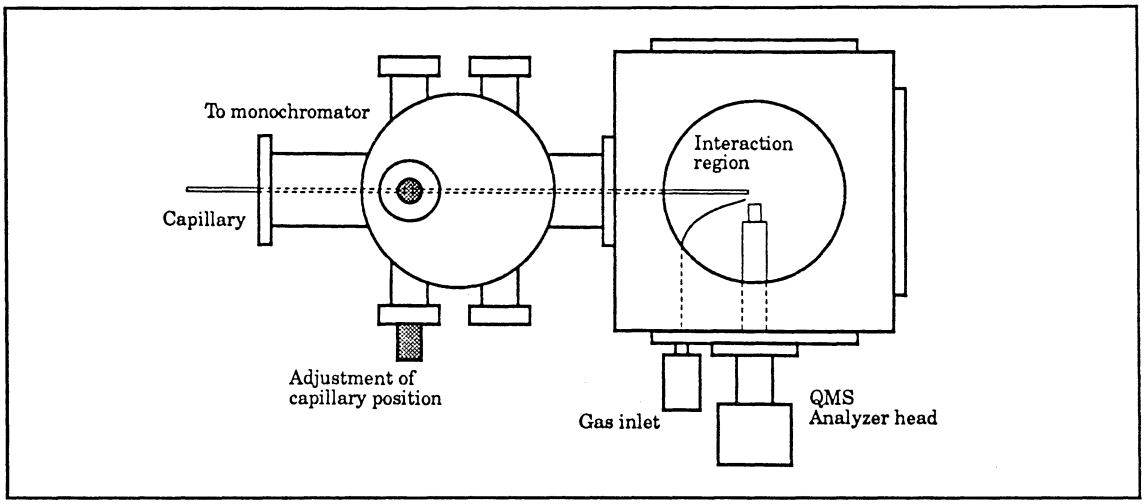

Fig. 1 The experimental set-up connected to the monochromator at beamline 52, as seen from above.

The use of glass capillaries for differential pumping in the VUV and X-ray regions has been reported by other groups [19, 20].

Both the long and narrow capillary and the exit slit contribute to a very low gas conductance into the monochromator. This is especially important since we use gases that can damage optical surfaces.

If the gas pressure in the experimental chamber is 10^{-4} mbar, the pressure would be typically about 10^{-7} mbar in the middle section and 10^{-8} mbar in the monochromator. The middle section is pumped by a cryo pump and the experimental chamber by a turbo-molecular pump.

The interaction region

Gas from a pressure bottle is injected in a thin jet in front of the end of the glass capillary. The jet is directed downwards, into the pump.

With two feed-throughs a GaAs photodiode and a fluorescent screen can be positioned in front of the capillary end. The fluorescent screen is an object glass covered with a thin layer of sedimented yttriumvanadate (YVO_4), giving red fluorescence. The screen can be used to monitor the beam of radiation from the capillary and it is useful when the position of the capillary is adjusted. The photodiode is used for flux measurements.

Detection of ions

The ions produced in the interaction region are analyzed with a quadrupole mass spectrometer (QMS) manufactured by VG Quadrupoles.

Ion transfer optics in the front end of the QMS analyzer head extracts the ions from the interaction region. Only ions having the mass-charge ratio specified on the QMS control unit will traverse the quadrupole mass filter and be detected by the channel electron multiplier in the interior of the QMS analyzer head.

The mass spectrometer can be set up in either analogue or pulse-counting mode. In analogue mode the current from the channeltron is proportional to the number of ions detected. In our experiment the ion production rate is low and the pulse-count mode is preferred; each ion reaching the channeltron will give rise to a large negative pulse that can be noise discriminated and counted.

Some similar experiments use time-of-flight (TOF) mass spectrometers. One advantage of a QMS is that both positive and negative ions can be detected with a very low background. Another argument for using a QMS is that a TOF experiment must be done in single bunch mode, i.e with only one filled electron bunch in the storage ring, due to timing requirements.

8. References

[1] D. H. Tomboulian and P. L. Hartman, *Phys. Rev.* **102**, 1423 (1956).

[2] E.-E. Koch, ed., *"Handbook on Synchrotron Radiation"*, North-Holland Publishing Company, Amsterdam, 1983.

[3] J. Schwinger, *Phys. Rev.* **70**, 798 (1946).

[4] J. Schwinger, *Phys. Rev.* **75**, 1912 (1949).

[5] J. Schwinger, *Proc. Nat. Acad. Sci. U.S.* **40**, 132 (1954).

[6] P. O. Nilsson, ed., *"MAX Laboratory, Progress Report III January 1987"*, Lund, 1987.

[7] W. Stiefler, *"Some Light From MAX"*, Lund, 1988.

[8] U. Karlsson, ed., *"Max Lab. Activity Report 1989"*, Lund, 1990.

[9] Å. Andersson, MAX Lab., private communication.

[10] J. A. R. Samson, *"Techniques of Vacuum Ultraviolet Spectroscopy"*, Wiley, New York, 1967.

[11] H. G. Beutler, *J. Opt. Soc. Am.* **35**, 311 (1945).

[12] U. Litzén, *"Spektroskopiska instrument"*, University of Lund, Lund, 1985.

[13] S. Huldt, *"Atomic Spectroscopy, University of Lund, Annual Report 1985"*, p. 83, Lund, 1986.

[14] B. R. Lewis, *Appl. Optics* **21**, 2523 (1982).

[15] H.-J. Hagemann, W. Gudat and C. Kunz,*"Optical Constants From the Far Infrared To the X-ray Region: Mg, Al, Cu, Ag, Au, Bi, C and Al_2O_3"*, DESY, Hamburg, 1974.

[16] *"Micro Controle, Catalogue 1985-86"*, Micro Controle, Evry (France), 1985.

[17] H. Oertel, H. Schenk and H. Baumgärtel, *Chem. Phys.* **46**, 251 (1980).

[18] T. Masuoka and J. A. R. Samson, *J. Chem. Phys.* **74**, 1093 (1981).

[19] U. Becker, *Vacuum* **38**, 597 (1988).

[20] R. H. Pantell and P. S. Chung, *Appl. Optics* **18**,897 (1979).

[21] S. Huldt and U. Litzén, *"Atomic Spectroscopy, University of Lund, Annual Report 1988"*, p. 56, Lund, 1989.